

Physics of nova outbursts: Theoretical models of classical nova outbursts with optically thick winds on $1.2 M_{\odot}$ and $1.3 M_{\odot}$ white dwarfs

Mariko KATO¹, Hideyuki SAIO,² and Izumi HACHISU³

¹Department of Astronomy, Keio University, Hiyoshi, Yokohama 223-8521, Japan

²Astronomical Institute, Graduate School of Science, Tohoku University, Sendai, 980-8578, Japan

³Department of Earth Science and Astronomy, College of Arts and Sciences, The University of Tokyo, 3-8-1 Komaba, Meguro-ku, Tokyo 153-8902, Japan

*E-mail: mariko.kato@hc.st.keio.ac.jp

Received ; Accepted

Abstract

We present time-dependent nova outburst models with optically thick winds for a $1.2 M_{\odot}$ and $1.35 M_{\odot}$ white dwarfs (WDs) with a mass accretion rate of $5 \times 10^{-9} M_{\odot} \text{ yr}^{-1}$ and for a $1.3 M_{\odot}$ WD with $2 \times 10^{-9} M_{\odot} \text{ yr}^{-1}$. The X-ray flash occurs 11 days before the optical peak of the $1.2 M_{\odot}$ WD and 2.5 days before the peak of the $1.3 M_{\odot}$ WD. The wind mass loss rate of the $1.2 M_{\odot}$ WD ($1.3 M_{\odot}$ WD) reaches a peak of $6.4 \times 10^{-5} M_{\odot} \text{ yr}^{-1}$ ($7.4 \times 10^{-5} M_{\odot} \text{ yr}^{-1}$) at the epoch of the maximum photospheric expansion with the lowest photospheric temperature of $\log T_{\text{ph}}$ (K)=4.33 (4.35). The nuclear energy generated during the outburst is lost in a form of radiation (61% for the $1.2 M_{\odot}$ WD; 47% for the $1.3 M_{\odot}$ WD), gravitational energy of ejecta (39%; 52%), and kinetic energy of the wind (0.28%; 0.29%). We found an empirical relation for fast novae between the time to optical maximum from the outburst t_{peak} and the expansion timescale τ_{exp} . With this relation, we are able to predict the time to optical maximum t_{peak} from the ignition model (at $t = 0$) without following a time-consuming nova wind evolution.

Key words: novae, cataclysmic variables — stars: interiors — stars: mass-loss — white dwarfs — X-rays: binaries

1 Introduction

A nova is a thermonuclear runaway event on a mass-accreting white dwarf (WD) (Priyalnik & Kovetz 1995; Kovetz 1998; Yaron et al. 2005; Epelstain et al. 2007; Shen et al. 2009; Denissenkov et al. 2013; Idan et al. 2013; Wolf et al. 2013; Kato et al. 2014; Kato et al. 2015; Tang et al. 2014; Tajitsu et al. 2015; Chen et al. 2019; José et al. 2020). Nova winds are accelerated owing to radiation pressure-gradient deep inside the photosphere (Friedjung 1966; Finzi & Wolf 1971; Żytkow 1972; Ruggles & Bath 1979). Stellar evolution codes, how-

ever, meet numerical difficulties in calculation beyond the extended stages of nova outbursts (Kato et al. (2017a) for a review). Kato et al. (2017b) showed, for the first time, a way how to calculate the whole cycle of nova outburst including radiative acceleration in a self-consistent way. Based on their results, Kato et al. (2022a) presented the classical nova model for a $1.0 M_{\odot}$ WD with a mass accretion rate of $\dot{M}_{\text{acc}} = 5 \times 10^{-9} M_{\odot} \text{ yr}^{-1}$. This is a unique nova model that self-consistently includes radiation-pressure-gradient acceleration in the outburst evolution calculation. The present work adds two more one cycle models of classical novae ($1.2 M_{\odot}$ and $1.3 M_{\odot}$ WDs), which enable us to

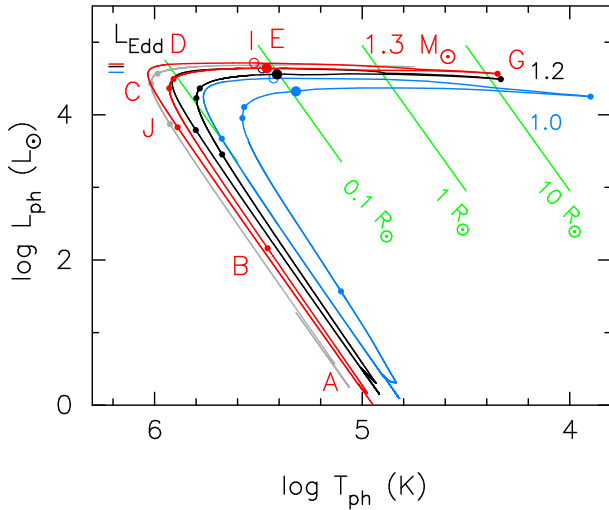


Fig. 1. The HR diagrams of one cycle of hydrogen shell flashes for our outburst models of $1.0 M_{\odot}$ (blue line), $1.2 M_{\odot}$ (black line), $1.3 M_{\odot}$ (red line), and $1.35 M_{\odot}$ (light gray) WDs. The $1.35 M_{\odot}$ model is shown only for the rising phase (up to before maximum expansion of the photosphere). Selected stages during a shell flash are denoted counterclockwise direction starting from the bottom of the cycle. A: Quiescent phase before the shell flash. B: The epoch when L_{nuc} reaches maximum ($t = 0$). C: Highest photospheric temperature in the rising phase. D: Peak of X-ray flash (0.3 keV - 1.0 keV). E: Wind begins to emerge from the photosphere. G: The maximum expansion when both the wind mass loss rate and photospheric radius reach maximum. I: The wind mass-loss stops (open circle). The supersoft X-ray phase starts. J: The supersoft X-ray luminosity (0.3 keV- 1.0 keV) decreases to one tenth of the maximum value. The short horizontal line indicates the Eddington luminosity (Equation (1)) for 1.3, 1.2, and $1.0 M_{\odot}$ WD models. The thick straight green lines show a locus of constant photospheric radius of $R_{\text{ph}} = 10, 1, 0.1, \text{ and } 0.01 R_{\odot}$.

quantitatively compare the nova outbursts for different WD masses.

This paper is organized as follows. Section 2 presents our models including X-ray light curves and internal structures. Section 3 reports energy budget in the nova outburst for each of our model. Discussion and concluding remarks follow in sections 4 and 5, respectively.

2 Nova models

We have calculated nova models of 1.2 and $1.35 M_{\odot}$ WDs accreting matter at a rate of $\dot{M}_{\text{acc}} = 5 \times 10^{-9} M_{\odot} \text{ yr}^{-1}$. The chemical composition of accreting matter is assumed to be solar, $X = 0.7$, $Y = 0.28$, and $Z = 0.02$. The mass accretion rate of $\dot{M}_{\text{acc}} = 5 \times 10^{-9} M_{\odot} \text{ yr}^{-1}$ is a typical value for classical novae (e.g., a central observed value of $\dot{M}_{\text{acc}} = 3 \times 10^{-9} M_{\odot} \text{ yr}^{-1}$ given by Selvelli & Gilmozzi (2019); or close to the center in the \dot{M}_{acc} distribution of galactic novae in Fig.6 of Hachisu et al. (2020)). With the $1.0 M_{\odot}$ model (Kato et al. 2022a), we have a set of three WD mass ($1.0, 1.2, \text{ and } 1.35 M_{\odot}$) for $\dot{M}_{\text{acc}} = 5 \times 10^{-9} M_{\odot} \text{ yr}^{-1}$. This enables us to see the dependence of nova prop-

erties on the WD mass, although only an early part of nova explosion is presented for the $1.35 M_{\odot}$. We also calculate a $1.3 M_{\odot}$ WD with $\dot{M}_{\text{acc}} = 2 \times 10^{-9} M_{\odot} \text{ yr}^{-1}$. We increased carbon mass fraction of the hydrogen-rich envelope by 0.1 and decreased helium mass fraction by the same amount, at the beginning of ignition, to mimic heavy element enhancements in ejecta, which are often observed in novae. This $X_{\text{C}} = 0.1$ model is one of the candidate models for YZ Ret that satisfy the observational duration of the short X-ray flash. Here, we have calculated a full cycle of the model. On the other hand, only a very early phase of nova outburst (the X-ray flash phase) is published in model EF of Kato et al. (2022c).

We calculate nova evolution with a Henyey-type evolution code in which the optically thick winds are consistently included as a boundary condition of the evolution calculation. We used the same computer code and calculation method as in Kato et al. (2022a); We stop the mass accretion when the photospheric luminosity L_{ph} increases to $\log L_{\text{ph}}/L_{\odot} = 3.5$ and resumes when the luminosity decreases less than $\log L_{\text{ph}}/L_{\odot} = 2.5$. We use the OPAL opacity tables (Iglesias and Rogers 1996).

More exactly, we first calculate several cycles of nova evolution with the Henyey-type code with temporarily assumed mass-loss rate as a function of time. Then we obtain the steady wind solution (Kato & Hachisu 1994) that fits smoothly to the interior structure at each step of evolution with mass loss. If the steady-state wind mass-loss rate deviates significantly from that assumed in the evolution calculation, we recalculate the whole evolution cycle with different mass-loss rate. We iterate this process until we have a steady wind solution that (1) fits smoothly to the inner structure and (2) the obtained wind mass-loss rate converges to the assumed value of the Henyey code. This iteration takes much human-time. In the $1.35 M_{\odot}$ WD model, this method does not work well in the extended stage of the outburst.

The model parameters are summarized in Table 1; the WD mass, mass accretion rate in quiescent phase, the carbon enhancement (C-mix), central temperature of the WD (T_{WD}), recurrence period, mass accreted until the thermonuclear runaway sets in (M_{acc}), ignition mass (M_{ig}), maximum temperature in the hydrogen nuclear burning layer through an outburst period, and maximum nuclear luminosity. The accreted mass is smaller than the ignition mass because there was leftover hydrogen-rich layer when the previous outburst had finished.

Among three models ($1.0 M_{\odot}$, $1.2 M_{\odot}$ and $1.35 M_{\odot}$ WDs) with $\dot{M}_{\text{acc}} = 5 \times 10^{-9} M_{\odot} \text{ yr}^{-1}$, the $1.0 M_{\odot}$ WD model is taken from Kato et al. (2022a). As the mass accretion rate and composition is the same, the main dif-

ference of these three models is the gravitational energy of the WD. More massive WDs ignite with smaller ignition masses because a stronger gravity yields a larger gravitational heating at the bottom of the hydrogen-rich envelope. Thus, thermonuclear runaway begins at a smaller ignition mass than in less massive WDs. As a result, the recurrence period is shorter in more massive WDs.

The last column in Table 1 shows the maximum nuclear burning rate $L_{\text{nuc}}^{\text{max}}$. The carbon enhanced model of the $1.3 M_{\odot}$ WD shows much larger $L_{\text{nuc}}^{\text{max}}$ than the others because hydrogen burning is accelerated by carbon enrichment through the CNO cycle.

2.1 H-R diagram

Figure 1 shows one cycle of shell flashes in the HR diagrams. It should be noted that the track of the $1.35 M_{\odot}$ model is not a full cycle but ended at $\log T$ (K)=4.75 in the pre-maximum/rising phase because of numerical difficulty. Before onset of the hydrogen shell flash, each accreting WD stays around the bottom of the loop (denoted by label A). After thermonuclear runaway sets in, the photospheric luminosity quickly increases keeping the photospheric radius almost constant. We define the onset of the shell flash ($t = 0$) by the time when L_{nuc} reaches maximum. This epoch is denoted by label B in Figure 1. After that, the nova evolves toward point C, where the photospheric temperature reaches maximum $T_{\text{ph}}^{\text{max}}$, and then toward point D (peak of X-ray flash). When the envelope further expands, optically thick winds begins to emerge from the photosphere at point E, and then the matter acceleration becomes stronger. This emergence of wind occurs at $\log T_{\text{ph}}$ (K) $\sim 5.2 - 5.3$, close to the Fe opacity peak (Iglesias and Rogers 1996). The photospheric radius attains its maximum and the wind mass loss rate also reaches maximum at point G. In the decay phase after point G, the nova track turns back to the left in the HR diagram. The photospheric radius decreases and the temperature T_{ph} increases with time. The winds stop at point I (open circle). The supersoft X-ray phase corresponds to the nova track from point I to point J, where the supersoft X-ray luminosity decreases down to one tenth of its maximum value. The time at each epoch is summarized in Table 2.

The Eddington luminosity defined by

$$L_{\text{Edd}} \equiv \frac{4\pi c G M_{\text{WD}}}{\kappa_{\text{el}}} \quad (1)$$

is indicated with short horizontal bars in the upper-left of Figure 1 for each WD mass, where $\kappa_{\text{el}} = 0.2(1 + X) \text{ g}^{-1} \text{ cm}^2$ is the electron scattering opacity and X is the hydrogen content. The photospheric luminosity hardly exceeds the Eddington luminosity and evolves horizontally before

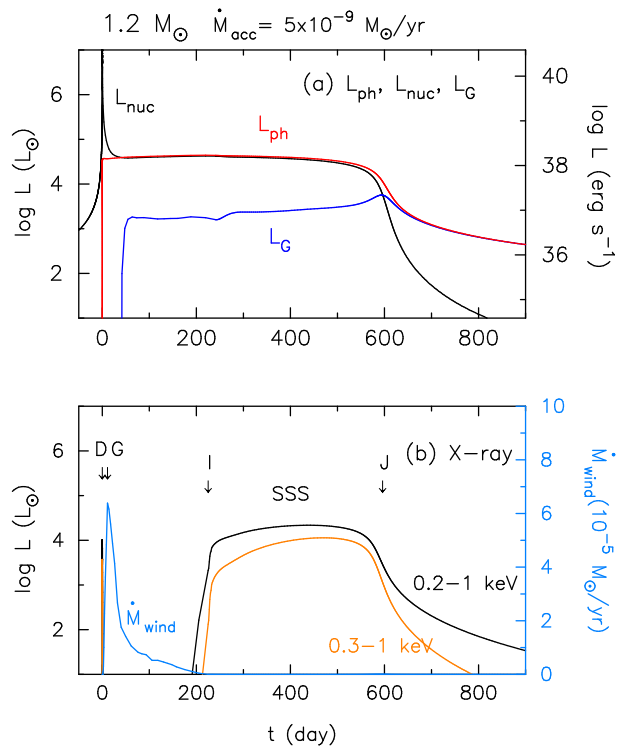


Fig. 2. (a) The temporal variations of the photospheric luminosity L_{ph} (red line), total nuclear burning energy release rate L_{nuc} (black line), and total gravitational energy release rate L_{G} (blue line) for the $1.2 M_{\odot}$ WD. We stopped the mass accretion at $t = 2.6 \times 10^{-4}$ day and restarted at $t = 1070$ day. (b) The supersoft X-ray light curves for the energy band of 0.2–1.0 keV (black line) and 0.3–1.0 keV (orange line). Time $t = 0$ corresponds to the epoch B in Fig.1. The four epochs are indicated by the four downward arrows: Epoch D (peak of X-ray flash), G (maximum photospheric expansion, i.e., peak of wind mass-loss rate), I (end of wind phase), and J (supersoft X-ray luminosity decreases to one tenth of its maximum).

and after the maximum expansion as already reported in Kovetz (1998) and Denissenkov et al. (2013).

2.2 Evolution of bolometric luminosity and X-ray light curve

Figures 2(a) and 3(a) show the temporal variations of the emergent bolometric luminosity L_{ph} , total nuclear energy release rate $L_{\text{nuc}} = \int \epsilon_{\text{nuc}} \delta m$, and integrated gravitational energy release rate $L_{\text{G}} = \int \epsilon_{\text{g}} \delta m$ for the $1.2 M_{\odot}$ and $1.3 M_{\odot}$ WDs, respectively. Here, ϵ_{nuc} and ϵ_{g} are energy generation rates per unit mass owing to nuclear burning and gravitational energy release, respectively, and $\int \delta m$ is the integration on the mass.

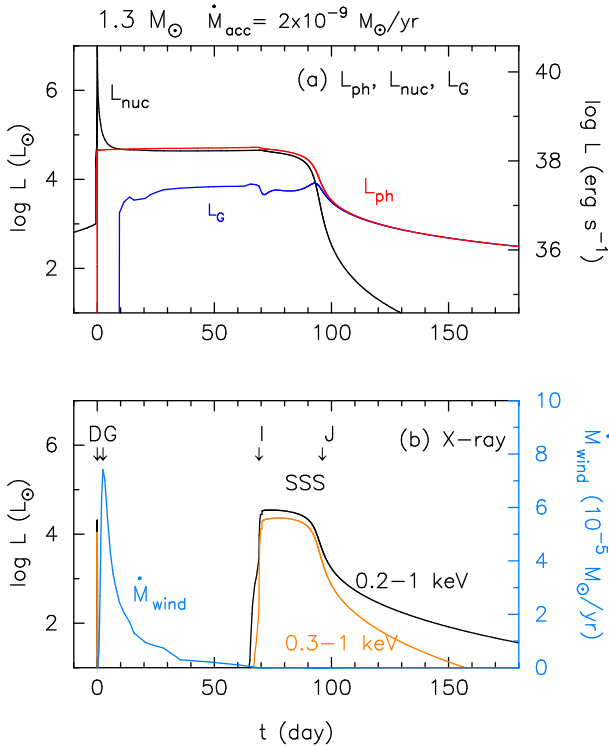
In the very beginning of the nova outburst, the nuclear energy generation rate L_{nuc} amounts $\log L_{\text{nuc}}/L_{\odot} = 9.65$ on the $1.3 M_{\odot}$ WD and 8.55 on the $1.2 M_{\odot}$ WD, which are much larger than each photospheric luminosity L_{ph} . A large amount of the generated energy is consumed to lift up the degeneracy, heat, and expand the envelope ($L_{\text{G}} < 0$)

Table 1. Characteristic properties of a shell flash model

model	M_{WD} (M_{\odot})	\dot{M}_{acc} ($M_{\odot} \text{ yr}^{-1}$)	C-mix	$\log T_{\text{WD}}$ (K)	P_{rec} (yr)	M_{acc} (M_{\odot})	M_{ig} (M_{\odot})	$\log T^{\text{max}}$ (K)	$\log L_{\text{nuc}}^{\text{max}}$ (L_{\odot})
M13C	1.3	2×10^{-9}	0.1	7.689	1000	2.00×10^{-6}	2.15×10^{-6}	8.24	9.65
M135	1.35	5×10^{-9}	0.	7.786	224	1.12×10^{-6}	1.27×10^{-6}	8.32	8.56
M12	1.2	5×10^{-9}	0.	7.730	1450	7.26×10^{-6}	8.24×10^{-6}	8.26	8.55
M10	1.0	5×10^{-9}	0.	7.687	5370	2.68×10^{-5}	3.04×10^{-5}	8.18	8.36

Table 2. Time since the beginning of the flash

Stage	B	C	D	E	F	G	I	J
	$L_{\text{nuc}}^{\text{max}}$	$T_{\text{ph}}^{\text{max}}$	X flash	wind starts	T5	max exp	wind ends	$0.1 L_{\text{X}}^{\text{max}}$
M13C10								
Time (d)	0.0	0.00073	0.0018	0.072	0.71	2.5	69	96
$\log T_{\text{ph}}$ (K)	5.46	5.93	5.91	5.46	5.00	4.35	5.52	5.89
M135								
Time (d)	0.0	0.0030	0.0095	0.25	–	7.2	–	–
$\log T_{\text{ph}}$ (K)	5.93	6.02	5.99	5.50	–	4.75	–	–
M12								
Time (d)	0.0	0.012	0.024	0.77	2.7	11	225	596
$\log T_{\text{ph}}$ (K)	5.674	5.80	5.78	5.41	5.00	4.33	5.48	5.80
M10								
Time (d)	0.0	0.063	0.11	1.05	2.83	26.0	530	6.46 yr
$\log T_{\text{ph}}$ (K)	5.10	5.58	5.57	5.32	5.01	3.90	5.43	5.68

**Fig. 3.** Same as those in Fig. 2, but for the $1.3 M_{\odot}$ WD. The mass accretion stopped at $t = 0$ and resumed on $t = 190$ day.

in the nuclear burning region. As a result, the net energy flux at the surface is less than the Eddington luminosity. The thermal energy is stored as the gravitational energy ($L_G < 0$) in the very early phase, but it is emitted later with a low luminosity, $0 < L_G \lesssim 0.1 L_{\text{ph}}$, as shown in Figures 2(a) and 3(a). Thus, the photospheric luminosity does not much exceeds the Eddington luminosity ($L_{\text{ph}} \lesssim L_{\text{Edd}}$).

Note that the super-Eddington luminosity is often observed in various nova outbursts (e.g., della Valle & Izzo (2020)), which is explained as the contribution of free-free emission from optically-thin plasma just outside the photosphere of a nova (Hachisu & Kato 2006; Hachisu & Kato 2015). However, this problem is beyond the scope of the present work. (See Figure 9 and equation (B3) of Hachisu & Kato (2023) for the $1.0 M_{\odot}$ WD.)

Figures 2(b) and 3(b) show the X-ray light curves calculated for the two energy bands of 0.2–1.0 keV and 0.3–1.0 keV, for the $1.2 M_{\odot}$ and $1.3 M_{\odot}$ WDs, respectively. Both the total nova duration (H-burning on) and the SSS phase are much shorter on the $1.3 M_{\odot}$ WD. The X-ray turn-on time, X-ray turnoff time, and the nova duration have been used to estimate the WD mass (Hachisu & Kato 2010; Wolf et al. 2013; Kato & Hachisu 2020; Hachisu et al. 2024).

The X-ray flux in figures 2(b) and 3(b) show two peaks. The earlier X-ray peak (X-ray flash) is slightly fainter than the later SSS phase, which is common among all the shell

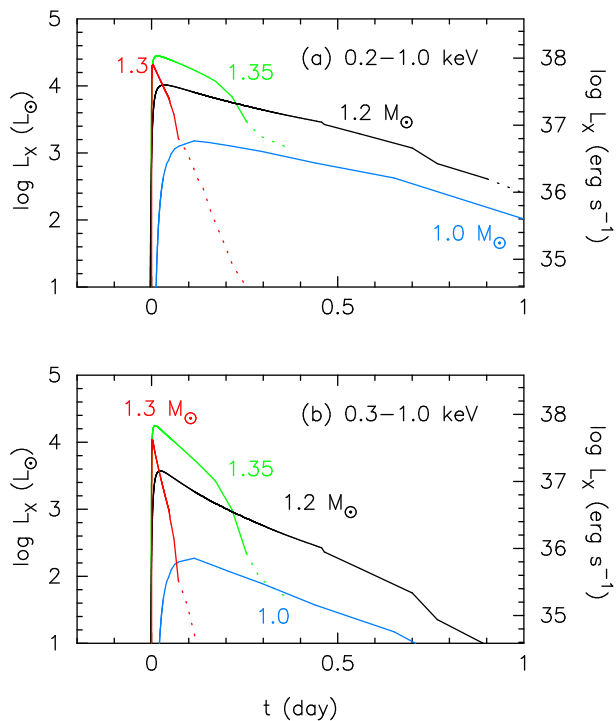


Fig. 4. Close up views of X-ray light curves during X-ray flashes in (a) energy band of 0.2–1.0 keV, and (b) 0.3–1.0 keV. The dotted part indicates the wind phase, where the X-ray flux may not be detected owing to self-absorption by the ejecta outside the photosphere. The $1.3 M_{\odot}$ WD model has the mass accretion rate of $\dot{M}_{\text{acc}} = 2 \times 10^{-9} M_{\odot} \text{ yr}^{-1}$ and an envelope which are mixed with carbon after hydrogen ignites. The other models, 1.35, 1.2, and $1.0 M_{\odot}$ WDs are for the same mass accretion rate of $5 \times 10^{-9} M_{\odot} \text{ yr}^{-1}$ with the solar composition envelope. The $1.0 M_{\odot}$ WD model is taken from Kato et al. (2022a), and $1.35 M_{\odot}$ WD model from Kato et al. (2022b).

flash models, because the maximum temperature and luminosity in the X-ray flash phase are lower than those in the SSS phase (see Fig. 1). The duration of the SSS phase is much longer than that in the X-ray flash phase. In the SSS phase, the nova evolves in a thermal timescale $L_{\text{ph}} \sim L_{\text{nuc}}$. On the other hand, the nuclear luminosity is much larger than the photospheric luminosity ($L_{\text{nuc}} \gg L_{\text{ph}}$) in the X-ray flash phase. The difference, $L_{\text{nuc}} - L_{\text{ph}}$, is mainly consumed to expand the envelope matter quickly, which terminates the high temperature stage in a short time.

2.3 X-ray flash

Figure 4 shows X-ray light curves during their X-ray flash phases for four different WD masses. The 0.2–1.0 keV band corresponds to the SRG/eROSITA instrument, and 0.3–1.0 keV does to the Swift/XRT. Because most of photons are emitted below 1.0 keV, the X-ray luminosity hardly changes even if we adopt a higher upper limit, e.g., 10 keV.

The peak flux is higher for more massive WDs be-

cause of higher photospheric temperature and luminosity as shown in Figure 1. The X-ray flash decays fastest in the C-rich $1.3 M_{\odot}$ WD model followed by the solar-composition models in the order of the 1.35, 1.2, and $1.0 M_{\odot}$ WDs.

Figure 4 demonstrates the dependence of the X-ray flux on the WD mass as well as the energy band. Less massive WDs show lower fluxes especially in the 0.3–1.0 keV band because a substantial part of the radiation is emitted below 0.2 keV. Thus, it is unlikely that X-ray flashes are detected in low mass WDs ($M_{\text{WD}} \lesssim 1.0 M_{\odot}$).

The recent detection of an X-ray flash in the classical nova YZ Ret (König et al. 2022) provides a rare opportunity to confirm theoretical models. The X-ray flash in YZ Ret was detected only once during the SRG/eROSITA all sky survey with four hours cadence, indicating that the X-ray flash lasted only briefly (< 8 hr). The blackbody temperature and luminosity is estimated to be $T_{\text{BB}} = 3.27^{+0.11}_{-0.33} \times 10^5$ K and $L_{\text{ph}} = (2.0 \pm 1.2) \times 10^{38} \text{ erg s}^{-1}$ (König et al. 2022), respectively. These properties suggest that the WD is very massive as examined by Kato et al. (2022b) and Kato et al. (2022c). Hachisu & Kato (2023) presented a theoretical model of YZ Ret, in which a $1.33 M_{\odot}$ WD reproduces the multiwavelength light curves, from early gamma-ray emission to later supersoft X-ray phase, as well as optical light curves.

From the X-ray spectrum analysis of YZ Ret, König et al. (2022) found no major intrinsic absorption during the X-ray flash. Thus, Kato et al. (2022b) concluded that (1) no dense matter exists around the WD photosphere, (2) no indication of a shock wave, and (3) the hydrogen-rich envelope is almost hydrostatic. Note that all of these are consistent with our theoretical model. Optically-thick winds do not yet emerge from the photosphere at the epoch of X-ray bright (X-ray flash) phase and the envelope is almost hydrostatic.

Our X-ray light curves in Figure 4 suggest that we can expect bright X-ray flash for massive WDs ($> 1.0 M_{\odot}$) before the optical brightening, except the WD is deeply embedded in a dense gaseous matter likely in symbiotic stars.

2.4 Internal structure of the envelope

Figures 5 and 6 show the temporal changes of the density and velocity profiles in the 1.2 and $1.3 M_{\odot}$ WDs, respectively, from an early stage to optical maximum (epoch G), and from optical maximum (G) to the end of the outburst (J). Convection occurs above the hydrogen burning zone (blue line region) from the beginning of thermonuclear runaway to the extended stages of nova envelope, and then

disappears shortly after epoch G.

Optically thick winds are accelerated to emerge from the photosphere when the photospheric temperature decreases and approaches the prominent Fe opacity peak at $\log T$ (K) ~ 5.3 . The velocity quickly increases around the critical point of the wind (Bondi 1952; Kato & Hachisu 1994), where the velocity reaches the sound velocity. We did not include convective energy transport above the critical point, because the wind velocity is supersonic and therefore convective eddies cannot turn back.

In the pre-maximum phase [Figures 5(c) and 6(c)] the acceleration region (around the opacity peak: $\log T$ (K) ~ 5.2) moves outward. As the envelope expands the radius at the critical point increase, the density of which also increases. Thus, the wind mass loss rate, $\dot{M}_{\text{wind}} = 4\pi r_{\text{cr}}^2 \rho_{\text{cr}} v_{\text{cr}}$, increases with time. The velocity reaches the terminal velocity deep inside the photosphere, because the winds are hardly accelerated outside the opacity peak.

In this way, the wind mass-loss rate increases, but the velocity at the photosphere decreases in the pre-maximum phase. On the contrary, in the post-maximum phase, the wind mass-loss rate decreases whereas the velocity at the photosphere increases with time. These trends are common among the three, i.e., $1.0 M_{\odot}$, $1.2 M_{\odot}$, and $1.3 M_{\odot}$ WD models.

Hachisu & Kato (2022) proposed a strong shock formation in the nova ejecta (so-called internal shock) based on the $1.0 M_{\odot}$ model (Kato et al. 2022a). Assuming that the ejecta motion is ballistic above the photosphere, they proposed a mechanism of strong shock formation outside the photosphere. In the pre-maximum phase, the later ejected matter has a smaller velocity so the ejected matter/gas expands. In the post-maximum phase, however, later ejected matter has a larger velocity that will catch up the earlier ejected matter, which causes a strong compression and then a shock. They predicted that a strong shock wave forms only after optical maximum.

This shock formation naturally explains hard X-ray emission (Friedjung 1987; Mukai & Ishida 2001) and absorption/emission line systems such as principal and diffuse-enhanced systems (McLaughlin 1942), as discussed by Hachisu & Kato (2022) and Hachisu & Kato (2023). Our 1.2 and $1.3 M_{\odot}$ WD models provide theoretical supports to the internal shocks for various fast novae.

Figure 6 also shows similar profiles, but for the $1.3 M_{\odot}$ WD model. The small hump in the velocity profile deep inside the critical point is caused by a small opacity peak owing to C and O at $\log T$ (K) ≈ 6.1 . Such a velocity hump does not appear in the 1.0 and $1.2 M_{\odot}$ WD models. Note that carbon is not enhanced in the envelopes of 1.2 and $1.0 M_{\odot}$ WD models.

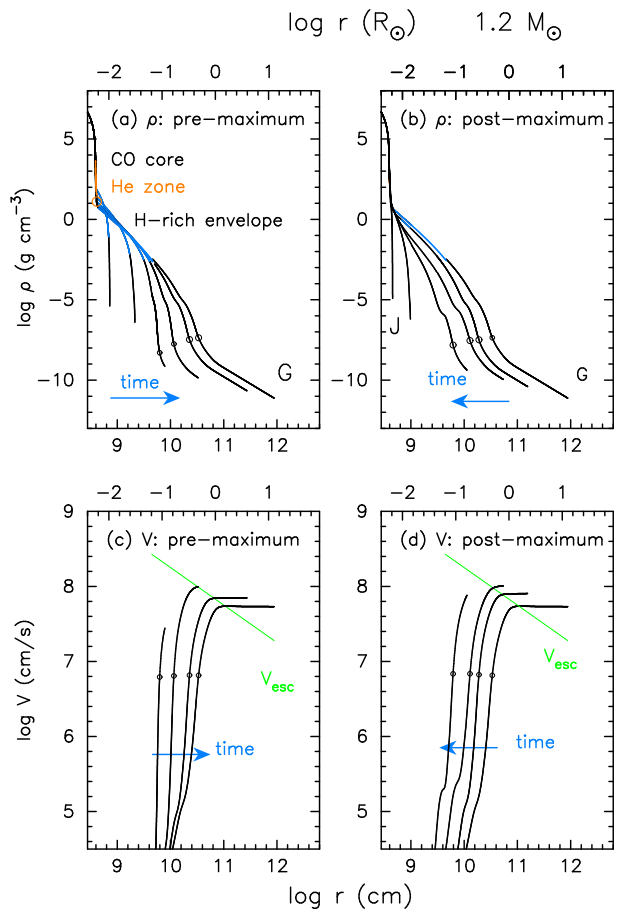


Fig. 5. Temporal structure changes in the $1.2 M_{\odot}$ WD model. The density profiles toward optical maximum (a) and after maximum (b). The velocity profiles toward optical maximum (c) and after maximum (d). Here, r is the radius from the center of the WD. The outermost point of each line corresponds to the photosphere. The blue lines indicate the convective region. The critical points of each wind solution are indicated by the small open black circles. The green straight line shows the escape velocity $v_{\text{esc}} = \sqrt{2GM_{\text{WD}}/r}$. In panel (a), the region of CO core is denoted by the black line while the helium layer is by the orange line. The open orange circle represents the place of maximum energy generation rate by nuclear burning $\epsilon_{\text{nuc}}^{\text{max}}$.

3 Energy budget

Figure 7(a) shows the internal structure of the envelope at epoch G of the $1.3 M_{\odot}$ WD model. The $1.2 M_{\odot}$ WD has a similar structure to that of the $1.3 M_{\odot}$ WD, and thus, we do not discuss it here. The local luminosity L_r is defined by the sum of radiative and convective luminosities, where r denotes the radius from the center of the WD. The local luminosity L_r steeply increases in the nuclear burning region, and then turns to decrease because a substantial part of L_r is absorbed above the zone. The convective region is indicated by the horizontal green line in Figure 7(a). The envelope is convective only in the innermost part, where L_r is large.

We plot in Figure 7(a) the local Eddington luminosity,

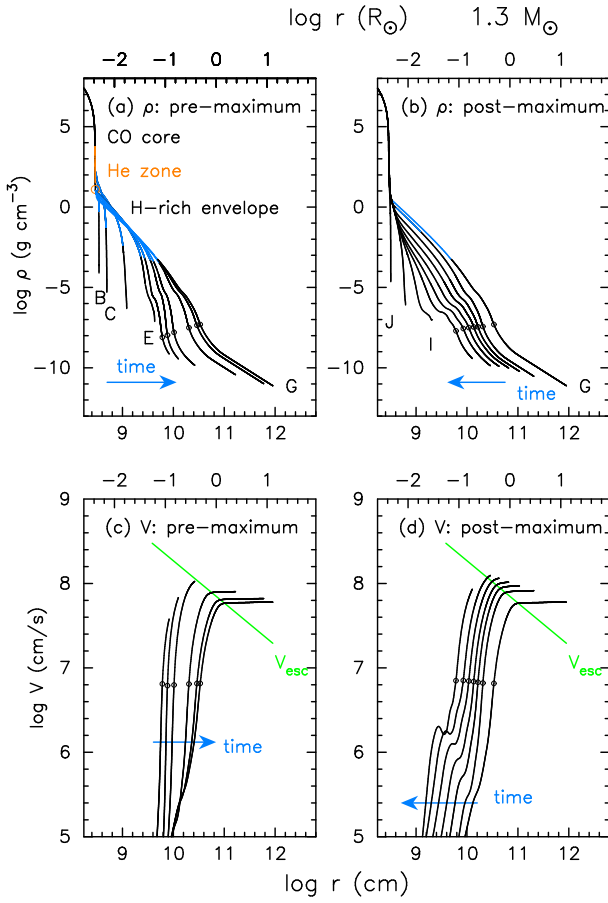


Fig. 6. Same as those in Figure 5, but for the $1.3 M_{\odot}$ WD model.

$$L_{\text{Edd},r} \equiv \frac{4\pi c G M_{\text{WD}}}{\kappa_r}, \quad (2)$$

where κ_r is the local opacity which is a function of the density and temperature for a given chemical composition. A small dip of $L_{\text{Edd},r}$ at $\log r$ (cm) ~ 10.1 in Figure 7(a) corresponds to a small peak in the opacity contributed by ionized C and O ($\log T$ (K) ~ 6.1 – 6.3) and a large dip of $L_{\text{Edd},r}$ at $\log r$ (cm) ~ 10.85 is caused by a large Fe peak at $\log T$ (K) ~ 5.2 . The wind is accelerated where the opacity increases outward and L_r exceeds the local Eddington luminosity $L_{\text{Edd},r}$ as shown in Figure 7(a).

During the wind mass-loss phase, the ejecta carry energy away from the WD. As introduced in Kato et al. (2022a), we integrated each term of the energy conservation equation, i.e.,

$$L_r - \dot{M}_{\text{wind}} \left(\frac{v^2}{2} + \omega_{\text{rad}} + \omega_{\text{gas}} - \frac{GM}{r} \right) = \Lambda, \quad (3)$$

and obtained each energy budget (Kato & Hachisu 1994). The second term in the left-hand-side of equation (3) is the energy carried with the moving matter, that includes the kinetic energy, enthalpy of radiation ω_{rad} (photon energy trapped in the moving matter), enthalpy of gas ω_{gas} , and gravitational energy.

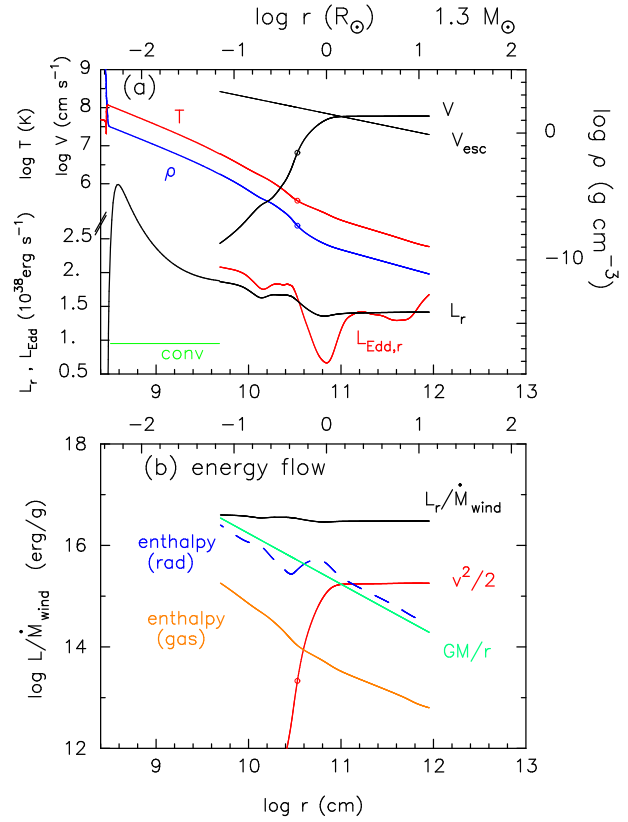


Fig. 7. Internal structure of the envelope at the maximum expansion of the photosphere (at epoch G) for the $1.3 M_{\odot}$ WD model. (a) The distribution of the temperature (red line), density (blue line), velocity (black), local luminosity L_r , and local Eddington luminosity. The outermost point of each line corresponds to the photosphere. The critical point of solar-wind type solution (Kato & Hachisu 1994) is indicated by open circle. (b) The distribution of the diffusive radiative luminosity per unit mass, $L_r/\dot{M}_{\text{wind}}$, and energy advected by winds: gravitational energy GM/r , radiation enthalpy (rad), gas enthalpy (gas), and kinetic energy $v^2/2$.

Figure 7(b) depicts the distribution of each energy flux divided by \dot{M}_{wind} . The enthalpy of radiation is decreasing outward to compensate the gravitational energy, and as a result, the diffusive luminosity $L_r/\dot{M}_{\text{wind}}$ becomes a dominant term near the photosphere. These properties are essentially the same as those of the $1.0 M_{\odot}$ WD model in Kato et al. (2022a).

The diffusive luminosity L_r substantially decreases outward at $\log r$ (cm) ~ 10.7 , where the opacity increases outward and therefore the local Eddington luminosity decreases outward. The decreased radiative energy flux is consumed for wind mass loss, supplying the gravitational energy of the envelope and kinetic energy of the winds.

Following Kato et al. (2022a), we estimate how much amount of nuclear energy is consumed to drive the wind mass-loss. We have calculated the total nuclear energy generated during one cycle of a nova outburst to be $E_{\text{nuc}} = \int L_{\text{nuc}} dt$, energy emitted as radiation from the pho-

Table 3. Energy budget

subject	E_{nuc}	M_{ej}	E_{rad}	E_{G}	E_{kin}
unit	(erg)	(M_{\odot})	(erg)	(erg)	(erg)
1.3 M_{\odot}	4.0×10^{45}	1.8×10^{-6}	1.9×10^{45}	2.1×10^{45}	1.2×10^{43}
%	100	–	47	52	0.29
1.2 M_{\odot}	1.4×10^{46}	6.7×10^{-6}	8.3×10^{45}	5.2×10^{45}	3.8×10^{43}
%	100	–	61	39	0.28
1.0 M_{\odot}	3.2×10^{46}	3.0×10^{-5}	2.1×10^{46}	1.1×10^{46}	7.3×10^{43}
%	100	–	64	35	0.23

tosphere $E_{\text{rad}} = \int L_{\text{ph}} dt$, and the kinetic and gravitational energy carried out in the wind $E_{\text{kin}} = \int \frac{1}{2} \dot{M}_{\text{wind}} v_{\text{ph}}^2 dt$, and $E_{\text{G}} = \int GM_{\text{WD}} \dot{M}_{\text{wind}} / R_0 dt$, respectively, where v_{ph} is the wind velocity at the photosphere and R_0 the radius of nuclear burning region, $\log(R_0/R_{\odot}) = -2.229$ for 1.2 M_{\odot} and $\log(R_0/R_{\odot}) = -2.365$ for 1.3 M_{\odot} .

Table 3 summarizes the energy budget for our models. The total nuclear energy E_{nuc} is smaller for a more massive WD, because the ignition mass is much smaller. Correspondingly each allocated energies are smaller for a more massive WD.

Most of the energy is used in the photospheric emission (blackbody emission) and gravitational energy of the wind. Even in the strong shell flash of the 1.3 M_{\odot} WD, the allocated kinetic energy is as small as less than 1% of the total nuclear energy.

4 Discussion

4.1 Pre-maximum evolution of fast novae

Pre-maximum evolution of a nova outburst has been poorly understood. For example, the timescale from the outburst to optical maximum, t_{peak} , is not well constrained for many novae, contrary to the decay timescales such as t_2 and t_3 , which are the days by 2 and 3 mag decay from the optical (V) maximum. Table 2 shows the evolution time from the ignition to the maximum expansion (stage G) to be $t_{\text{peak}} = 26$ day in model M10 (1.0 M_{\odot}) and 11 day in M12 (1.2 M_{\odot}). Although M135 model has stopped before reaching stage G because of numerical difficulties, we estimate the time to stage G to be $t_{\text{peak}} \sim 7$ day. In these models, the WDs accrete matter of the same chemical composition ($X = 0.7$, $Y = 0.28$, and $Z = 0.02$) at the same mass-accretion rate of $\dot{M}_{\text{acc}} = 5 \times 10^{-9} M_{\odot} \text{ yr}^{-1}$. For the carbon enhanced model M13C10 ($\dot{M}_{\text{acc}} = 2 \times 10^{-9} M_{\odot}$), the time from the ignition to stage G is as short as 2.5 day as expected from the short total duration of the outburst. We can see a tendency that the time to optical maximum is longer in a less massive WD (or shorter in a more massive WD).

It is difficult to observationally detect when the outburst begins. Many novae have been discovered near their optical peaks (stage G). Only the exception is the classical nova YZ Ret (König et al. 2022) in which an X-ray flash was detected for the first time, after unsuccessful attempts for other novae (Morii et al. 2016; Kato et al. 2016). The X-ray flash begins immediately after the thermonuclear runaway (see Table 2), and lasts only less than one day (Figure 4).

In YZ Ret, the time of optical peak is not well constrained but less than four days after the X-ray flash. The WD mass is estimated as massive as $\gtrsim 1.3 M_{\odot}$ from multiwavelength light curve fitting (Hachisu & Kato 2023). This short timescale ($t_{\text{peak}} \lesssim 4$ day) is consistent with the decreasing tendency of t_{peak} for a more massive WD in Table 2.

To formulate the tendency of t_{peak} , we define the timescale τ_{exp} of expansion of the envelope at point B (maximum nuclear burning rate) by

$$\tau_{\text{exp}} L_{\text{nuc}}^{\text{max}} = \frac{GM_{\text{WD}}}{R_{\text{WD}}} M_{\text{env}}, \quad (4)$$

where M_{env} is the envelope mass at ignition, i.e., $M_{\text{env}} = M_{\text{ig}}$, and R_{WD} is the WD radius and we adopt $R_{\text{WD}} = R_0$ at the radius of the bottom nuclear burning region. This relation presents an approximate balance between the nuclear energy released during the expansion and the work needed to lift-up the gravitational energy of the envelope accumulated before ignition.

We plot the $\log t_{\text{peak}} - \log \tau_{\text{exp}}$ diagram in Figure 8. Our four models, M10, M12, M135, and M13C, are located almost on a straight blue line in the diagram. Thus, our expansion timescale τ_{exp} defined by Equation (4) correctly indicates the time to the optical (V) peak t_{peak} , independently of the envelope chemical composition, mass-accretion rate, or WD mass. This means that we predict t_{peak} if we calculate $L_{\text{nuc}}^{\text{max}}$, $R_{\text{WD}} = R_0$, and $M_{\text{env}} = M_{\text{ig}}$ at the very early phase of nova outburst. From the straight line in Figure 8 we obtain the relation;

$$t_{\text{peak}} \approx 33 \left(\frac{\tau_{\text{exp}}}{\text{day}} \right)^{0.4} \text{ day}. \quad (5)$$

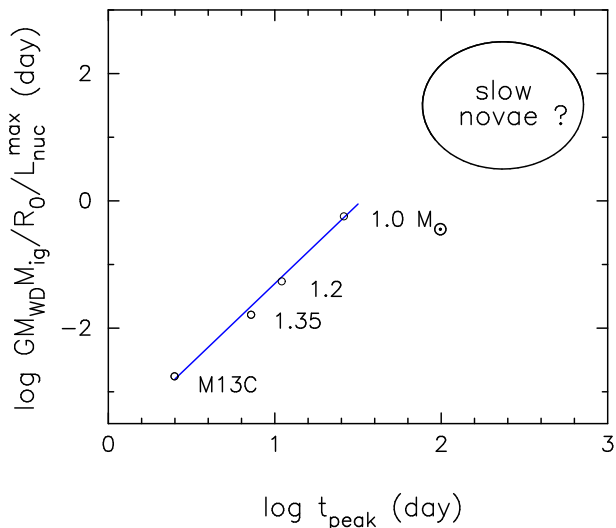


Fig. 8. The expansion timescale (τ_{exp}) versus time to the optical peak (t_{peak}) for fast novae, where $\tau_{\text{exp}} \equiv GM_{\text{WD}} M_{\text{ig}} / R_0 / L_{\text{nuc}}^{\text{max}}$ from Equation (4). The blue line has a slope of $t_{\text{peak}} \propto (\tau_{\text{exp}})^{0.4}$.

These $L_{\text{nuc}}^{\text{max}}$, R_0 , and M_{ig} are relatively easily obtained without computing very expanded stages such as stage G and, as a result, τ_{exp} is also easily obtained with our Henyey code because no winds are accelerated yet at point B.

4.2 Pre-maximum evolution of slow novae

Pre-maximum phases have been partly observed in some slow novae. In the extremely slow nova PU Vul, the m_{pv} brightened from 11.2 to 9.55 mag during 127 days (Wenzel 1979). The WD mass in PU Vul is estimated, from the UV 1455Å light curve fitting in the optical decay phase, to be about $0.6 M_{\odot}$ (Kato et al. 2011). In the slow nova CN Cha, it takes 300 days to rise from $V = 16$ to $V = 10$ (Lancaster et al. 2020). The WD mass is estimated to be about $0.57\text{--}0.6 M_{\odot}$ (Kato, & Hachisu 2023). In the slow novae V723 Cas, it took 24 days to rise from unfiltered CCD magnitude 12.2 to 9.2 (Ohshima et al. 1995). The WD mass possibly as small as $0.6\text{--}0.7 M_{\odot}$ (Kato & Hachisu 2011). For nova Vel 2022 (Gaia22alz), the g magnitudes rose from 17.8 to 13 in 100 days (Aydi et al. 2023). The WD mass is not known but the light curve resembles to the slow nova V723 Cas. We have no information on the outburst (ignition) time of these novae, but thermonuclear runaway should occur before the optical brightening. Thus, the duration between the onset of the outburst and the optical peak should be longer than these 23 - 300 days. It is probably a few hundred days or more for less massive WD ($\sim 0.6 M_{\odot}$). Such a long duration is consistent with the tendency in the lower mass limit in Table 2 and in Figure 8.

5 Concluding remarks

Novae show rich variety in their timescales, peak luminosities, speed classes, light curve shapes, spectral developments, ejecta properties etc. Such variety is a consequence of various WD masses, mass accretion rates, and binary parameters. To reveal the overall picture of nova phenomena, multiwavelength observations, along different stages of a nova outburst, play essential roles. Very early rising phase of a nova is an unexplored field, which has just been opened by the detection of an X-ray flash in YZ Ret. Our full-cycle shell flash models provide information of such a very early phase of a nova outburst which could be helpful in the massive survey era.

References

- Aydi, E., Chomiuk, L., Mikołajewska, J., Brink, J., Metzger, B.D. et al. 2023, MNRAS, 524, 1964,
 Bondi, H. 1952, MNRAS, 112, 195
 Chen, H.-L., Woods, T. E., Yungelson, L. R., Piersanti, L., Gilfanov, M., & Han, Z. 2019, MNRAS, 490, 1678
 della Valle, M., & Izzo, L. 2020, The Astronomy and Astrophysics Review, 28, 3,
 Denissenkov, P. A., Herwig, F., Bildsten, L., & Paxton, B. 2013, ApJ, 762, 8
 Epelstain, N., Yaron, O., Kovetz, A., & Prialnik, D. 2007, MNRAS, 374, 1449,
 Finzi, A., & Wolf, R. A. 1971, A&A, 11, 418
 Friedjung, M. 1966, MNRAS, 132, 317
 Friedjung, M. 1987, A&A, 180, 155
 Hachisu, I., & Kato, M. 2006, ApJS, 167, 59
 Hachisu, I., & Kato, M. 2010, ApJ, 709, 680
 Hachisu, I., & Kato, M. 2015, ApJ, 798, 76
 Hachisu, I., & Kato, M. 2022, ApJ, 939, 1,
 Hachisu, I., & Kato, M. 2023, ApJ, 953, 78
 Hachisu, I., Kato, M., & Matsumoto, K. 2024, ApJ, 965, 49
 Hachisu, I., Saio, H., Kato, M., Henze, M., & Shafter, A. 2020, ApJ, 902, 91,
 Idan, I., Shaviv, N. J., & Shaviv, G. 2013, MNRAS, 433, 2884
 Iglesias, C. A., & Rogers, F. J. 1996, ApJ, 464, 943
 José, J., Shore, S.N., Casanova, J. 2020 A&A, 634, A5,
 Kato, M., & Hachisu, I., 1994, ApJ, 437, 802
 Kato, M., & Hachisu, I., 2011, ApJ, 743, 157,
 Kato, M., & Hachisu, I. 2020, PASJ, 72, 82
 Kato, M., & Hachisu, I. 2023, ApJ, 951, 128,
 Kato, M., Hachisu, I., Cassatella, A., & González-Riestra, R. 2011, ApJ, 727, 72,
 Kato, M., Hachisu, I., & Saio, H. 2017a, in Proc. Palermo Workshop on The Golden Age of Cataclysmic Variables and Related Objects IV, PoS(GOLDEN 2017), ed. F. Giovannelli et al. (Trieste: SISSA), 56
 Kato, M., Saio, H., & Hachisu, I. 2015, ApJ, 808, 52
 Kato, M., Saio, H., & Hachisu, I., 2017b, ApJ, 838, 153
 Kato, M., Saio, H., & Hachisu, I. 2022a, PASJ, 75, 1005
 Kato, M., Saio, H., & Hachisu, I. 2022b, ApJL, 935, L15

- Kato, M., Saio, H., & Hachisu, I. 2022c, RNAAS, 6, 258
- Kato, M., Saio, H., Hachisu, I., et al. 2014, ApJ, 793, 136
- Kato, M., Saio, H., Henze, M. et al. 2016, ApJ, 830, 40
- König, O., Wilms, J., Arcodia, R., et al. 2022, Nature, 605, 248
- Kovetz, A. 1998, ApJ, 495, 401
- Lancaster, L., Greene, J. E., Ting, Y-S., et al. 2020, ApJ, 160, 125,
- Li, K.-L., Metzger, B. D., Chomiuk, L., et al. 2017, Nature Astronomy, 1, 697,
- McLaughlin, D. B. 1942, ApJ, 95, 428,
- Mukai, K., & Ishida, M. 2001, ApJ, 551, 1024,
- Morii, M., Yamaoka, H., Mihara, T., Matsuoka, M., & Kawai, N. 2016, PASJ, 68, S11,
- Ohshima, O., Kosaka, K., Hurst, G. M., Collins, M., Bortle, J. E., Kiss, L., Schmeer, P. 1995, IAU Circ., 6214, 4
- Prialnik, D., & Kovetz, A. 1995, ApJ, 445, 789
- Rugles, C. L. N., Bath, G. T., 1979, A&A, 80, 97
- Selvelli, P., & Gilmozzi, R. 2019, A&A, 622, A186
- Shen, K.J., Idan, I., & Bildsten, L. 2009, ApJ, 705, 693
- Tajitsu, A., Sadakane, K., Naito, H., Arai, A., Aoki, W. 2015, Nature, 518, 381,
- Tang, S., Bildsten, L., Wolf, W. M., et al. 2014, ApJ, 786, 61
- Wenzel, W. 1979, IBVS, 1608, 1
- Wolf, W. M., Bildsten, L., Brooks, J., & Paxton, B. 2013, ApJ, 777, 136 ; Erratum 782, 117
- Yaron, O., Prialnik, D., Shara, M.M., & Kovetz, A. 2005, ApJ, 623, 398,
- Żytkow, A. 1972, Acta Astronomy, 22, 103